Int. J. Heat Mass Transfer. Vol. 33, No. 7, pp. 1521–1533, 1990
Printed in Great Britain

0017–9310/90 $3.00 + 0.00

Local forced convective heat transfer from protruding and flush-mounted two-dimensional discrete heat sources

A. B. McENTIRE† and B. W. WEBB
Department of Mechanical Engineering, Brigham Young University, Provo, UT 84602, U.S.A.

(*Received* 12 *December* 1988 *and in final form* 6 *October* 1989)

Abstract—Experiments are undertaken to measure the local forced convective heat transfer characteristics of an array of two-dimensional discrete heat sources. Air flow rates yielding effective channel Reynolds numbers in the range from 1000 to 10000 are employed. Flush-mounted and protruding heater configurations are investigated in the study. Two different channel wall spacings independent of the heat source protrusion are also studied. Local temperature measurements are made along the uniformly heated surface parallel to the flow direction. The results of the experiments show that protruding heat sources yield higher heat transfer than flush-mounted heat sources at the same channel Reynolds number. The interruption of the thermal boundary layer in the adiabatic sections between the heaters results in heat transfer enhancement. Heat source protrusion yields significantly higher heat transfer rates for the second and subsequent heater for channal Reynolds numbers above 2000. This is explained in terms of a separated flow and vena contracta effect, with eventual downstream transition to turbulent flow, and is borne out by flow visualization experiments. The local heat transfer measurements reveal significant variation in wall temperature across the heater faces, which is strongly affected by the flow structure. Average heat transfer coefficients calculated by spatially integrating the local measurements are correlated and presented in terms of Reynolds number and the dimensionless geometric parameters studied.

INTRODUCTION

THE AREA of heat transfer from discrete heat sources has become a subject of increased interest in the last decade because of advances in the electronics industry. New generations of electronic devices are appearing which are faster, however at the expense of increased power dissipation. Miniaturization of electronic devices has also increased the heat flux density beyond that encountered traditionally in previous electronics technology. Thermal packing engineers in the electronics industry are becoming increasingly aware of the need for fundamental comprehension of the heat transfer characteristics of discretely heated, protruding energy dissipation elements. The thermal management issue requires that device junction temperatures be maintained below ceilings set by reliability considerations. This has spawned increased interest in the fundamental mechanisms of fluid flow and heat transfer in discrete heating situations. It is in response to this need that this study has been undertaken.

Heat transfer characteristics of discretely heated protrusions in forced convection situations have been treated to some extent in the literature. Sparrow *et al.* [1] studied experimentally the transport characteristics of an array of discrete protrusions in channel flow. The naphthalene sublimation technique was employed, with one active cube being placed in different configurations relative to the remainder of protuberances in the array. Forced convection from two-dimensional surface-mounted repeating ribs in the transitional flow regime has been studied [2]. It was found that the level of turbulence in the channel was well correlated with a Reynolds number based on the streamwise heater length. The influence of streamwise spacing and length of the two-dimensional heat transfer modules in a forced convective flow was also investigated [3]. The strong influence of channel height on average heat transfer from discretely heated protrusions in channel flow has also been demonstrated [4–6]. This is attributed to different hydrodynamic flow patterns. Biber and Sammakia [7] heated a single protrusion in an array, while measuring the temperature distribution. The effect of periodically varying heating was studied in a cylindrical tube [8]. Although the cylindrical geometry is not strictly relevant to the electronics cooling problem, the finding that the presence of thermally inactive zones between the active zones results in heat transfer enhancement is relevant to the problem considered here.

Recently, the problem of forced convection from discretely heated components has received attention from the analytical perspective as well. Laminar flow and conjugate heat transfer across three identical two-dimensional rectangular protruding blocks was analyzed using a finite difference method [9]. Local and average component Nusselt numbers were presented for several channel Reynolds and fluid Prandtl

† Currently at Boeing Airplane Co., Renton, WA 98057, U.S.A.

NOMENCLATURE

b	distance between the heater and opposing adiabatic wall, Fig. 1
D_h	effective channel hydraulic diameter, equation (2)
E_b	blackbody emissive power
F_{k-j}	radiation configuration factor
Gr^*	modified heat source Grashof number, $g\beta q_{conv}L^4/kv^2$
h	local convective heat transfer coefficient, equation (3)
k	thermal conductivity
L	streamwise length of the heater surfaces
Nu	local Nusselt number, hL/k
$\overline{Nu}$	average Nusselt number based on inlet temperature, equation (7)
$\overline{Nu}_b$	average Nusselt number based on bulk temperature, equation (10)
q_{cond}	local correction for conjugate heat flux in heater
q_{conv}	local convective heat flux from the discrete heater, equation (4)
q_{rad}	local radiation heat flux from heater surfaces
q_{Ohm}	Ohmic dissipation flux in heated foil
Re	Reynolds number based on the effective flow area, equation (1)
T_0	channel inlet temperature
T_w	local heater temperature
$\bar{u}$	average velocity in the effective channel flow area
w	spanwise width of the heater and channel
x	coordinate along the heater surface.

Greek symbol

ε	heater surface emissivity.

Subscripts

1, 2, 3, 4	indicates discrete heat source number, 1 being the first streamwise heater.

numbers. Periodically fully-developed flow and heat transfer over three-dimensional rectangular protrusions was also studied numerically using a finite difference technique [10]. As with the predictions of ref. [9], the highest local Nusselt numbers along the protrusion were found near the leading edge of the face oriented parallel to the flow direction. The study also revealed under what conditions a two-dimensional analysis is capable of predicting accurately the heat transfer characteristics of the three-dimensional system. Numerical predictions have been made for periodically fully-developed turbulent flow and heat transfer in two-dimensional ducts with rectangular protrusions [11, 12]. The k–ε turbulence model was employed to account for turbulent transport in the system. Predictions showed good agreement with the experimental results of ref. [3].

Although there has been considerable prior work on heat transfer from discrete heat sources in forced convective flow, the local heat transfer characteristics of the modules has received little attention. This is particularly true in considering the interaction of the thermal wake from one heater to the next. Additionally, the combined hydrodynamic and thermal entry regions of channels with flush-mounted and protruding discrete heat sources has received very little research attention. Most of the previous work has dealt either with a single heater in an array of otherwise thermally inactive protuberances, or average heat transfer from multiple heated sources, for the most part in the periodically fully-developed regime. It stands to reason that significant temperature gradients in the discretely heated modules may adversely affect the reliability and life of devices in electronic equipment. Hence, the objective of the present study was to obtain local heat transfer data for discretely heated two-dimensional sources in channel flow. The experiments were designed to coincide with modern electronic and communications equipment in geometric and Reynolds number similarity.

EXPERIMENTS

Experimental apparatus

An experimental setup was designed to accommodate the study of local heat transfer from discrete heat sources in forced convective flow. Data were collected on an array of four heat sources, each capable of continuously variable protrusion into the channel. Channel wall spacing was also variable. The following describes in detail the experimental apparatus and instrumentation used in the study.

The flow channel consisted of a smooth inlet, test section, and exit section, as shown in Fig. 1. The inlet section was fabricated from contoured extruded polystyrene covered with smooth Mylar plastic. The inlet was matched exactly to the channel so that added turbulence was minimized. The spanwise dimension of the test channel was 25.4 cm, adequately wide to assume a two-dimensional flow for the channel wall spacings studied here. One of the channel walls was designed so as to accommodate variable protrusion heat sources with adiabatic streamwise intervals in between. An adiabatic opposing channel wall was simulated with a 15.24 cm thickness of extruded polystyrene. The polystyrene surface exposed to the air

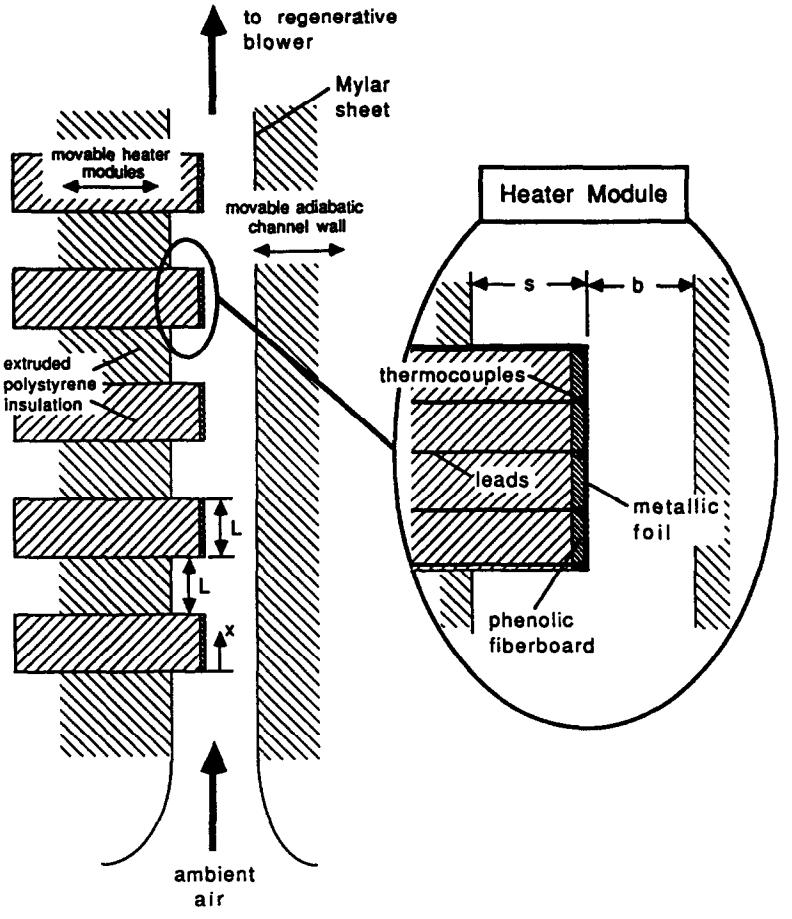

FIG. 1. Schematic of flow channel and discrete heat sources.

flow was covered with a 0.01 cm thick sheet of Mylar to provide a smooth channel boundary and to provide a radiatively black surface, the advantage of which will be shown in a later section. The adiabatic opposing wall was secured by a threaded rod extending through milled horizontal grooves in the spanwise bounding walls, which were constructed of Lexan to provide visual access. The grooves allowed the adiabatic channel wall to be moved relative to the wall on which the heat sources were mounted. Sixteen copper–constantan thermocouples were affixed to the insulated wall through the insulation and just beneath the Mylar surface at 2.54 cm vertical intervals starting at the channel inlet. Information from these temperature measurements enabled the calculation of the radiative heat loss from the discrete heat sources on the opposing wall.

The wall containing the discrete heat sources was made of a 38.1 cm length of 5.1 cm thick styrofoam insulation attached to a rigid Lexan substrate. This insulation slab was sectioned to house the discrete heat source modules. The first of five horizontal slots, 1.27 cm long in the streamwise direction, was machined 7.62 cm from the channel entrance, with subsequent identical slots spaced at 1.27 cm intervals. The heater modules were constructed so as to slide directly into these five slots.

The discrete heating modules were made $L = 1.27$ cm long in the flow direction and designed so as to provide variable protrusion into the channel. Each heater module consisted of a strip of 0.00254 cm thick stainless steel shim stock, 1.27 cm long in the streamwise direction, attached by epoxy adhesive to a 0.16 cm thick strip of phenolic fiberboard of the same streamwise length (see Figs. 1 and 2). The phenolic fiberboard, the same material used in printed circuit boards, was chosen because of its rigidity, ability to withstand elevated temperatures, and relatively low thermal conductivity. Five holes were drilled at equal streamwise intervals in the spanwise center of the phenolic substrate before the foil heaters were attached. Copper–constantan thermocouples made of small diameter wire (0.0127 cm diameter) were epoxied in these holes with the beads against the heated surfaces, as shown in Fig. 1. Despite efforts to insure intimate thermal contact during heater assembly, experiments revealed that significant thermal resistance existed between several of the thermocouple beads and the heated foil. This was particularly evident with thermocouples at the trailing edge of the heaters, where

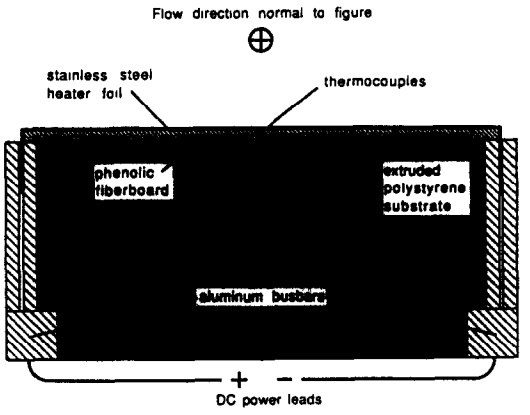

FIG. 2. Horizontal cross-sectional view of heat source modules. Flow direction is normal to the page.

relatively low convective heat transfer resulted in conjugate heat transfer effects which amplified the measurement error. Temperature data from these thermocouples were therefore discarded.

The composite stainless steel foil–phenolic substrate assembly described in the preceding paragraph was attached to polystyrene insulation sections which had been cut to fit snugly in the five slots milled in the heater wall. Thermocouple wires were drawn from the heated surfaces through a small gap in the insulation at its spanwise center, and out the back of the test section. The heater modules were fabricated such that they could be slid horizontally in and out of the slots in the polystyrene wall, providing for the study of variable protrusion into the flow channel.

The clear nature of the Lexan which constituted the bounding walls at the spanwise extremities of the channel permitted flow visualization with smoke generated by passing an electrical current through a horizontal, spring-loaded wire at the channel inlet. Glycerin was used to generate the smoke.

Electrical power was supplied to the stainless steel foil heaters through bus bars running the streamwise length of the channel. These bus bars consisted of two 2.54 cm aluminum rods of square cross-section, and were located behind the insulation which formed a portion of the partially heated channel wall. The heater foil was sandwiched between small aluminum blocks rigidly connected to the bus bars at either side of the test channel, as shown in Fig. 2. The foil heaters therefore formed a parallel electrical circuit.

Electrical power was supplied to the bus bars with a 20 V, 120 A d.c. source with voltage and current stable to 0.01%. The Ohmic dissipation in each of the five heaters was determined from the voltage–current product at the heated surface. The total current was displayed to 0.01 A by the power supply, while the voltage drop was measured with voltage taps attached to the foil heaters. The Ohmic dissipation was thus measured to an estimated accuracy of 2%. Typical heat fluxes imposed in the experiments were approximately 850 W m^{-2}. The Ohmic dissipation was found to be the same in each of the five heaters to within 3%.

Laboratory air was drawn through the test section by operating a regenerative blower in suction mode. The blower was driven by an electric motor with continuously variable control. Three rotameters of different ranges with calibrated accuracy of 5% were used to measure the air flow rate. The channel inlet air temperature was measured with a single thermocouple located near the inlet. The channel exit temperature was measured just upstream of the flowmeters to correct flow rates for deviations from calibration conditions.

Thermocouple voltages were read to 1 μV and software-compensated to yield temperatures in degrees Celsius. Data were acquired and stored for later data reduction. Flow visualization was performed and recorded with a 35 mm camera on Kodak Tri-X ASA 400 film by back-lighting the smoke generated using the setup described above.

An estimate of the uncertainty in the experimental data to be reported was made using standard techniques for single-sample measurements [13]. The propagation of the uncertainties into the dimensionless parameters was then determined. This study revealed an uncertainty in local Nusselt number of 7.6%, while the uncertainty in Reynolds number was estimated to be 8.9%.

Data reduction

The air flow rate in the channel was quantified by the Reynolds number, which was based on the velocity in the restricted flow area, b, as done previously [1]. The Reynolds number is

$$Re = \rho \tilde{u} D_h / \mu \tag{1}$$

where the hydraulic diameter is as defined conventionally for the effective flow area, and may be stated for the geometry studied as

$$D_h = \frac{2b}{(1+b/w)}. \tag{2}$$

The temperatures measured during each experiment were converted to local heat transfer coefficient using the following:

$$h = q_{conv}/(T_w - T_0) \tag{3}$$

where the convective heat flux, q_{conv}, was calculated by correcting the Ohmic heating in the foil for conduction and radiation losses

$$q_{conv} = q_{Ohm} - q_{cond} - q_{rad}. \tag{4}$$

Some recent investigators have based the local heat transfer coefficient on the inlet temperature, T_0 [2, 3, 6, 7]. Other approaches, however, have employed the local bulk or adiabatic wall temperature [4, 5]. The effect of the two choices on average heat transfer will be further explored in a subsequent section. The

Ohmic heating in the foil was calculated from the total energy dissipated and the area of each heater. The radiation losses were determined by assuming that the heater surfaces were diffuse gray. The opposing Mylar-covered wall was justifiably assumed to be radiatively black. The heater surfaces and opposing adiabatic wall were subdivided into regions over which the temperature was considered spatially uniform. The 16 temperature measurements made along the adiabatic wall were interpolated to give finer resolution there. Under the framework of these assumptions, the local radiant heat flux, $q_{\text{rad},k}$, from each heater may be determined from a simple summation as

$$q_{\text{rad},k} = \varepsilon \left[E_{bk} - \sum_{j=1}^{N} E_{bj} F_{k-j} \right] \tag{5}$$

where the subscript k denotes the heater location of interest, and the summation over j indicates the radiative heat loss to the N spatial subdivisions along the adiabatic opposite wall. A value of $\varepsilon = 0.17$ in keeping with available data for stainless steels [14] was used in the data reduction. In all experiments, the local correction for radiation loss never exceeded 6% of the Ohmic dissipation, q_{Ohm}.

Estimates revealed that the conduction heat loss was minimal. However, conjugate effects in the foil and phenolic substrate of each heater resulted in some lateral redistribution of the Ohmic dissipation. A simplified, one-dimensional conduction model was used to correct for this phenomenon. Each discrete heat source was divided into control volumes in the streamwise direction, and an energy balance was performed on each. The conjugate heat transfer correction accounted for the total Ohmic dissipation lost by conduction through the back of the insulation substrate (which was shown to be negligible), through the sides as conjugate heat transfer to adjacent control volumes, or by convection to the flowing fluid. The measured local temperatures were used to determine the net conduction heat transfer between control volumes on the interior of the heaters. At the leading and trailing edges of the heaters it was assumed that the heat transfer coefficient at the exposed heater face prevailed locally over the sides of the protrusions. The sensitivity of this assumption was assessed, revealing that the estimate of the local heat transfer coefficient there had only a minor effect on the correction for conduction redistribution. The correction for conduction amounted to a maximum of 6% of the Ohmic dissipation on the interior of the heater surface. However, there was more uncertainty in the estimates for the nodes surrounding the thermocouples at the two streamwise extremities of the heater. It is estimated that the conduction correction at the edges may amount to as much as 20% of the Ohmic heating in the foil, q_{Ohm}.

Once the convective heat flux had been determined from the corrected Ohmic dissipation according to equation (4), the local Nusselt number was determined according to

$$Nu = hL/k. \tag{6}$$

Note that the heat source length in the streamwise direction, L, has been used as the characteristic length in the local Nusselt number. The average Nusselt number over each heat source is also a relevant parameter, and is determined from the equation

$$\overline{Nu} = \bar{h}L/k \tag{7}$$

where the average heat transfer coefficient is determined by integrating the local heat transfer over the heater area

$$\bar{h} = \frac{1}{L} \int_0^L h(x)\, \mathrm{d}x. \tag{8}$$

In calculating the average heat transfer coefficient from the experimental data, the integral of equation (8) was approximated numerically. The local heat transfer coefficients were weighted by a fraction of the heater area (length) associated with each measurement. This area was equal to one-fourth the heater surface area for the three thermocouple measurement locations on the streamwise interior of the heater, and one-eighth of the heater area for the thermocouples located at the heater upstream and downstream edges. The thermophysical properties in the Reynolds and local and average Nusselt numbers were based on the inlet temperature, T_0.

EXPERIMENTAL RESULTS

The experimental test matrix was designed to investigate the heat transfer characteristics of discretely heated two-dimensional heat sources under conditions which closely approximate those employed in the electronics industry. Three different values of the heat source protrusion, s, were investigated, those being 0 (flush-mounted), 0.635, and 1.27 cm. This represents the range of dimensionless discrete heater protrusions of $0 \leqslant s/L \leqslant 1.0$. Additionally, experiments were performed for two effective channel spacings, $b = 0.635$ and 1.27 cm, corresponding to dimensionless heater-wall spacings, b/L of 0.5 and 1.0. In all experiments, the streamwise spacing between heat sources was equal to the heat source length, L. Seven different air flow rates for each geometric configuration were employed, yielding nominal channel Reynolds numbers in the range of 1000 to 10000. Experiments were performed only for air ($Pr = 0.72$) as the cooling fluid. Local and average heat transfer results are presented in the sections to follow characterized by these dimensionless parameters. The maximum buoyancy parameter, Gr^*/Re^2, in all experiments performed was 0.11, suggesting that the flow and heat transfer were forced convection dominated.

Flush-mounted heater configuration

The local Nusselt number along the four heater surfaces is shown in Fig. 3 for five nominal Reynolds numbers ranging from 1000 to 10000 for the flush-mounted heater configuration, $s/L = 0$, with dimensionless channel wall spacing $b/L = 1.0$. The local heat transfer decreases monotonically from a maximum at the leading edge along each of the four heaters. This is indicative of a growing thermal boundary layer along each of the discrete heaters. There is a significant variation in heat transfer over each heater. The variation in local Nusselt number over the heater face ranges from 25 to 90%. The resulting temperature gradient could conceivably have a significant impact on the life and reliability of electronic devices.

Figure 3 reveals that the Nusselt number at the leading edge of all heaters is slightly higher than that at the trailing edge of the preceding heater. The presence of the adiabatic sections between the heaters interrupts the thermal boundary layer and results in an increase in the local Nusselt number. Hydrodynamic and thermal mixing occurs in the adiabatic sections separating the heaters. This results in a more uniform temperature profile in the fluid approaching each of the discrete heat sources than would be found in a continuously-heated channel. If the wall heating were uniform and uninterrupted across the range $0 \leqslant x/L \leqslant 8$, and barring a transition to turbulent flow, the heat transfer behavior would be expected to follow generally the local Nu profile along heater 1, then continue to decrease below the values shown for the subsequent three heaters. The enhancement due to the presence of thermally inactive zones between the heated sections amounts easily to 100% of what Nu would be for the continuous (uninterrupted) heating. This level of enhanced transport has been shown previously for hydrodynamically developed turbulent flow in tubes with non-uniform heating at the duct wall [8].

Figure 3 shows generally that as the Reynolds number is increased, the local Nusselt number along each heater also increases. For example, the local Nusselt number for the $Re = 5000$ flow is approximately 100% higher than for the $Re = 1000$ flow along corresponding heaters. This is in keeping with the theory for hydrodynamically and thermally developing channel flow; the local Nusselt number in a duct is higher at a given axial location for higher channel Reynolds numbers. There is some evidence of a transition to turbulent flow and heat transfer for the higher Reynolds number flows in the flush-mounted configuration data of Fig. 3. This may be seen in the local Nu profiles for $Re \geqslant 5000$. The local Nusselt number at the leading edge of heater 3 ($x/L = 4$) is greater than the local Nusselt number at the corresponding leading edge location on the preceding heater ($x/L = 2$). This observation is made only for the higher Reynolds number experiments. The wall surface roughness and inherent discontinuities in the channel wall at the heater locations will undoubtedly govern the location of this transition. As will be illustrated in a subsequent section, the presence of protruding heat sources greatly accelerates this transition both spatially and in terms of the critical Reynolds number for this case where the flow is developing hydrodynamically.

Figure 4 illustrates the heat source average Nusselt number calculated according to equations (7) and (8) for the flush-mounted heat source configuration. Also shown are the coefficients of a least-squares curve fit of the average Nusselt number data for a correlation of the form

$$\overline{Nu} = A\, Re^{m}. \tag{9}$$

The correlation coefficient, R^2, for all of the curve fits was 0.99 or higher. The results of the figure corroborate the observations made for the flush-mounted configuration local Nusselt number data of Fig. 3. It is also noted that an increase in the channel Reynolds number results in an increase in the average Nusselt number, the dependence for the flush heaters being approximately proportional to $Re^{0.4}$. Again, for this repeatedly redeveloping thermal boundary layer, the

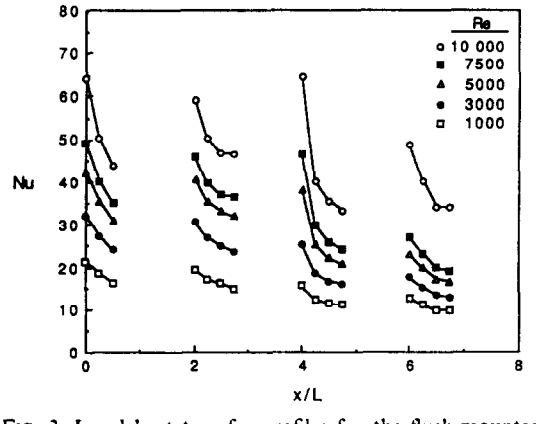

FIG. 3. Local heat transfer profiles for the flush-mounted heat sources, $s/L = 0$, $b/L = 1.0$.

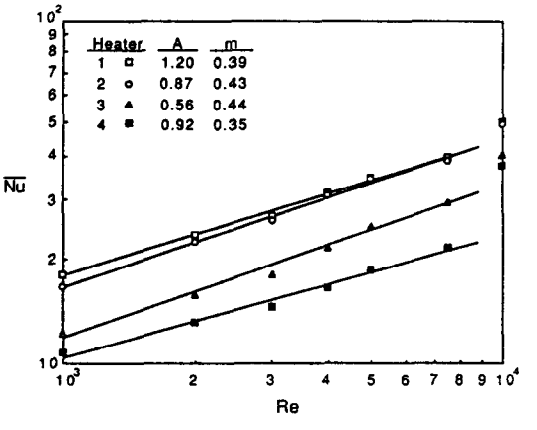

FIG. 4. Variation of the average discrete heat source Nusselt number with Reynolds number for the flush-mounted heater configuration, $s/L = 0$, $b\ L = 1.0$

Reynolds number dependence is quite different from the accepted average Nusselt number relation for fully-developed turbulent flow in continuously heated channels and ducts, which varies with $Re^{0.8}$. The average Nusselt number data for $Re = 10000$ were not used in the curve fit since there seemed to be an indication of transition to turbulent flow for the highest Re studied. These $Re = 10000$ data are, however, plotted in Fig. 4 for comparison. It is clear that a mechanism for substantially increased $\overline{Nu}$ is present in the highest Re data, as is seen by their stark departure from the lower Reynolds number data correlations. The augmentation in $\overline{Nu}$ due to the onset of turbulent flow is highest for the final heater where the average Nusselt number data for $Re = 10000$ are 70–80% higher than for $Re = 7500$. Heater 4 is the furthest downstream and its heat transfer characteristics are most likely to be impacted by a transition to turbulent flow and heat transfer.

Effect of heat source protrusion

As stated previously, the local and average heat transfer were characterized for several different nonzero values of the dimensionless heat source protrusion, s/L. These results are presented and contrasted in sections to follow. The general impact of heat source protrusion on the heat transfer behavior will be investigated by contrasting these results with those presented in Figs. 3 and 4 for flush-mounted heater assemblies.

Figure 5 illustrates the local Nusselt number profiles along the four heaters at five Reynolds numbers corresponding to those presented for the flush-mounted configuration in Fig. 3. Note that the Reynolds number has been defined with a hydraulic diameter based on the effective channel flow area, b, and the corresponding average velocity, $\bar{u}$, through the restrictions formed by the heaters and the opposite channel wall. Hence, comparing data for identical Reynolds numbers but different dimensionless geometric parameters b/L and s/L appropriately yields the same average fluid velocity in the channel section at each heater. Figure 5 shows the same general local Nusselt number behavior along the face of each heater: (1) increased channel Reynolds number yields higher local heat transfer along the face of each heater, (2) the maximum heat transfer occurs at the leading edge of each heater, and (3) the local heat transfer decreases monotonically with increasing streamwise distance. The variation in local Nusselt number across the face of each heater is greater at higher Reynolds number. However, the percentage change in Nu is roughly the same from the leading to the trailing edge of the heated surfaces for all Reynolds numbers.

There is one interesting contrast between the protruding heat source data of Fig. 5 and the flush-mounted data of Fig. 3. At Reynolds numbers approximately greater than 3000, the local Nusselt number for the second and subsequent heaters are all higher than the local Nusselt number along heater 1. This trend toward higher Nu is accentuated at the highest Reynolds numbers studied. For example, the local Nusselt number along heater 2, Nu_2, is approximately 90% higher than Nu_1 at corresponding streamwise locations along the face of each heater. Also noticed is the fact that the local Nusselt number profiles along the second, third and fourth heaters are in general, higher than that found along the face of heater 1. This is at variance with what was observed for the flush-mounted heater configuration. The increased heat transfer characteristics exhibited for the $s/L = 0.5$, $b/L = 1.0$ data of Fig. 5 over the $s/L = 0$, $b/L = 1.0$ data of Fig. 3 may be explained by flow separation and associated vena contracta, with possible vortex shedding at the first heater. This flow instability leads to an eventual downstream transition to turbulent flow above $Re \approx 2000$. This instability in the flow structure resulting from the constriction at the first heater is a precursor to transition. This will be demonstrated more clearly in flow visualization photographs to follow.

Figure 6 compares in more detail the local heat

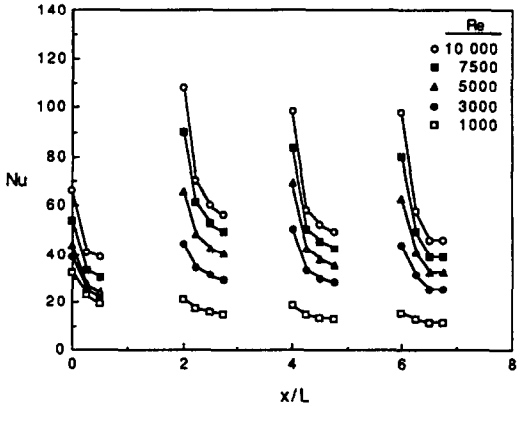

FIG. 5. Local heat transfer characteristics along the discrete heat sources as a function of Reynolds number for $s/L = 0.5$, $b/L = 1.0$.

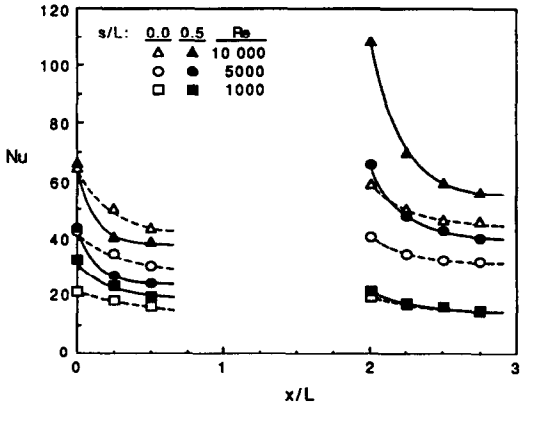

FIG. 6. Detailed comparison of the local Nusselt number along the first and second heater for the protruding ($s/L = 0.5$) and flush-mounted ($s/L = 0$) configurations at $b/L = 1.0$.

transfer data along heaters 1 and 2 for the flush-mounted and protruding heater configurations for $Re = 1000$, 5000 and 10000. The figure reveals that Nu is very nearly the same for both geometric configurations along heater 1. Surprisingly, the protruding heat sources ($s/L = 0.5$) exhibit local heat transfer along heater 1 which is 10–30% lower than Nu_1 for the flush-mounted heaters ($s/L = 0$) over most of the heat transfer area except for the lowest Reynolds number, $Re = 1000$. For $Re = 1000$, the Nu_1 distribution along the protruding heat source is 20–50% higher than the corresponding flush-mounted Nu_1 data. In stark contrast to the data for heater 1, the local heat transfer along heater 2 for the $s/L = 0.5$ configuration are 30–90% higher than the $s/L = 0$ data except for the low Reynolds number case. For $Re = 2000$, the data for $s/L = 0$ and 0.5 are almost identical.

The representation of Fig. 6 illustrates quite graphically the influence of separation and vena contracta effect on the heat transfer at the first heater. Flow visualization using the glycerin-generated smoke technique outlined briefly in the description of the experimental apparatus revealed that the transition to turbulent flow for the geometric parameters corresponding to those of Figs. 5 and 6 occurred near $Re = 1500$. Figures 7(a) and (b) illustrate the streaklines as revealed by the ribbon of glycerin smoke for two Reynolds numbers, 1000 and 2000, respectively. The $Re = 1000$ flow structure (Fig. 7(a)) is clearly laminar with very little interaction between the flow in the unobstructed core and the cavities formed by the protruding heat sources. The single ribbon of smoke prevails throughout the test section, indicating that laminar flow and heat transfer are expected. A sharp contrast to the flow structure of Fig. 7(a) for $Re = 1000$ is seen in Fig. 7(b), where the Reynolds number has been increased to 2000 for the same geometry. The formation of a vena contracta at heater 1 is evident in the photograph; the flow clearly separates at the leading edge of heater 1, and is deflected toward the opposite channel wall. This flow structure is similar at the second heater, although further breakup of the smoke ribbon is observed. The instability in the flow caused by the heaters leads to an eventual transition to turbulent flow and heat transfer, as evidenced by the complete breakup and mixing of the smoke ribbon further downstream. There is now considerable interaction of the core flow with the protruding heaters and the associated adiabatic cavities. These flow visualization results are qualitatively similar to those presented previously [2, 3] for geometrically different protrusions but for the same Reynolds number range.

The local Nusselt number data of Fig. 5 were integrated to determine the average Nusselt number for each heater for the geometric configuration $s/L = 0.5$, $b/L = 1.0$. The results of the calculation are shown graphically in Fig. 8. Also shown are the correlations for the Reynolds number dependence of $\overline{Nu}$ for heaters 2–4 in the Reynolds number range $2000 \leqslant Re \leqslant 10000$. The correlation was of the form of equation (9). No attempt was made to correlate the average Nusselt number data of heater 1, since the complex flow fields depended very strongly on Reynolds number. The inability of a correlating equation to accurately represent the $\overline{Nu}$ data of heater 1 is seen readily in the figure. Heaters 2–4 correlate very well with a power law dependence on the Reynolds number. Note that the Reynolds number dependence of $m \approx 0.53$ is substantially higher than the $m \approx 0.4$ dependence observed for the flush-mounted heater assembly. Additionally, the average Nusselt numbers as reflected by the correlations are all substantially higher than those seen in Fig. 4 for the $s/L = 0$ data. Note also that the $\overline{Nu}$ data for $Re = 1000$ are lower than that reflected by the least-squares correlations extrapolated to the lower Reynolds number for heaters 2–4. It is again obvious in the $\overline{Nu}$ data that the transition to turbulent flow demonstrated by both the local Nusselt number data of Figs. 5 and 6 and the flow visualization of Fig. 7 yields higher heat transfer for $Re \geqslant 2000$.

The local heat transfer results for further increases in the heat source protrusion ($s/L = 1.0$ for $b/L = 1.0$) are shown in Fig. 9. Note that with the same b/L as for the data of Fig. 5, the effective flow area between heat source and opposite channel wall is the same. The data are in general, similar to the heat transfer results for $s/L = 0.5$ in Fig. 5, with higher heat transfer at heaters downstream of heater 1. One observation of great interest is the presence of a local maximum in Nu downstream of the leading edge of heater 1 for high Reynolds numbers. This phenomenon was not observed in the $s/L = 0.5$ results. This may be explained by a reattachment of separated flow along the face of heater 1 near $x/L \approx 0.2$. The separated flow yields low Nu at $x/L = 0$, with higher Nu observed at the point of reattachment. This phenomenon has been observed previously in turbulent flow in circular ducts [15]. The separated flow was not observed for $s/L = 0.5$ because the heat source did not protrude far enough into the channel to cause the flow at heater 1 to deflect significantly. The average Nusselt numbers corresponding to the Nu data of Fig. 9 for $s/L = 1.0$ and $b/L = 1.0$ will be presented in the next section.

The effect of heat source protrusion on the average heat transfer relative to the flush-mounted heat source results may be summarized in Table 1. The correlations of average Nusselt number along the four heaters for $s/L = 0.5$ and 1.0 (for a given wall spacing, $b/L = 1.0$) have been normalized by the least-squares correlation for the flush-mounted configuration, $\overline{Nu}_{fm}$. Such a normalization reveals the extent of heat transfer enhancement along each of the four heaters due to their protrusion. The results of Table 1 indicate that there is always enhancement in heat transfer for the protruding heat sources for the Reynolds number range studied for both $s/L = 0.5$ and 1.0. This enhancement ranges from over 30% at $Re = 2000$ to

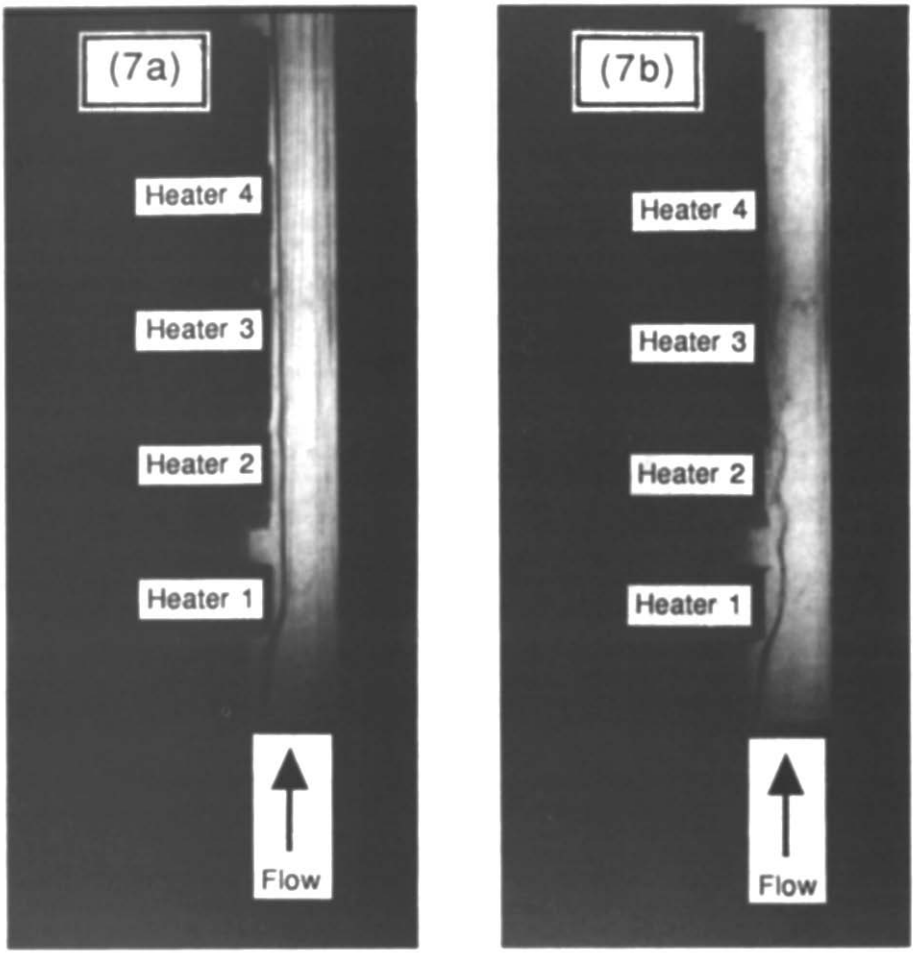

FIG. 7. Photographic results of flow visualization for $s/L = 0.5$, $b/L = 1.0$: (a) $Re = 1000$; (b) $Re = 2000$. Flow direction is from bottom to top.

nearly 300% for $Re = 10\,000$. The results also show that there is little increase in $\overline{Nu}$ when the heat source protrusion is increased from $s/L = 0.5$ to 1.0. The maximum increase in the average Nusselt number is only 17% for an increase in the protrusion of the heat source from $s/L = 0.5$ to 1.0. It appears that once the heaters are protruding far enough into the channel to result in modification of the flow structure, further protrusion yields only a minor change in the average heat transfer characteristics.

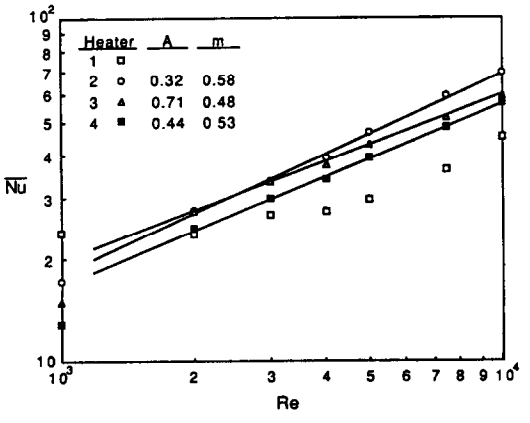

FIG. 8. Average Nusselt number data corresponding to the local Nusselt number data of Fig. 5 for $s/L = 0.5$, $b/L = 1.0$.

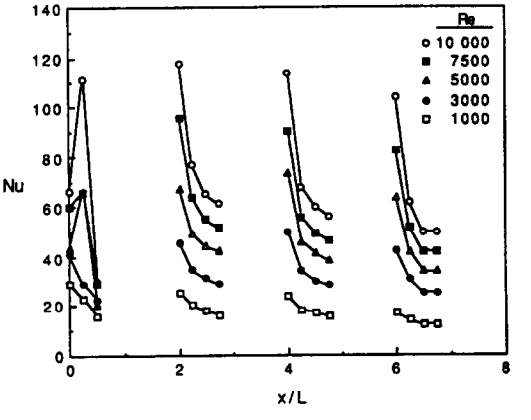

FIG. 9. Local Nusselt number profiles for $s/L = 1.0$, $b/L = 1.0$.

Table 1. Ratio of correlated protruding heat source average Nusselt number to the flush-mounted $b/L = 1.0$ data ($\overline{Nu}_{fm}$) for heaters 2–4

s/L	$(\overline{Nu}/\overline{Nu}_{fm})_2$	$(\overline{Nu}/\overline{Nu}_{fm})_3$	$(\overline{Nu}/\overline{Nu}_{fm})_4$
0.5	$0.37\,Re^{0.19}$	$1.27\,Re^{0.04}$	$0.48\,Re^{0.18}$
1.0	$0.39\,Re^{0.16}$	$1.04\,Re^{0.08}$	$0.39\,Re^{0.21}$

Effect of wall spacing

The influence of the effective flow area, measured by the dimensionless geometric parameter b/L, was investigated for a given heat source protrusion, s/L. Figure 10 shows the local Nusselt number distributions along the discrete heat sources as a function of Reynolds number. This figure may be contrasted with Fig. 5, which showed data for the same dimensionless heat source protrusion ($s/L = 0.5$) but for a larger flow area, $b/L = 1.0$. The same transition to turbulent flow is shown downstream of the first heater in Fig. 10, which results in substantially increased Nu for the second and subsequent heaters at higher Reynolds numbers. However, it may be seen that for a given Reynolds number, the local heat transfer data for $b/L = 0.5$ (Fig. 10) are 25–60% higher than the $b/L = 1.0$ case (Fig. 5). For a given Reynolds number, both cases have the same volumetric flow rate. However, the average fluid velocity is nearly twice as high for the more restricted flow of the $b/L = 0.5$ assembly. These higher velocities are responsible for the increased local heat transfer in the channel with more restriction and the data which are shown in Fig. 10. There appears to be an anomalous rise in the local heat transfer for $Re = 10\,000$ along heater 1 near the trailing edge. This may be due to the superposition of the core flow passing through the channel near the opposite wall with a secondary impingement of the flow deflected away by the heater itself, and redirected toward the heater by the opposite channel wall.

The average heat transfer corresponding to the data of Fig. 10 are shown in Fig. 11. The coefficient and exponent of the correlating equation, equation (9), are shown in the figure for heaters 2–4. Again, these $s/L = 0.5$, $b/L = 0.5$ results may be compared to the $s/L = 0.5$, $b/L = 1.0$ data of Fig. 8. The Reynolds number dependence of the average Nusselt number for the $s/L = 0.5$ heater assembly is approximately $m \approx 0.65$, whereas the corresponding dependence for $s/L = 1.0$ is $m \approx 0.55$. The dependence on Re as revealed by the correlations for $s/L = 0.5$, $b/L = 0.5$ is similar to the $m \approx 0.65$ dependence observed previously [3] for periodically fully-developed turbulent flow and heat transfer from protruding discrete heat sources. A direct comparison could not be made since the geometric parameters studied in that study were not identical to those investigated here. As was observed for the local heat transfer behavior, the average heat transfer coefficients are higher as well for the $b/L = 0.5$ case. The extent of heat transfer enhancement along the heaters due to a decrease in the effective channel flow area (decrease in b/L) may be assessed by comparing the magnitude of the correlated average Nusselt number for the $b/L = 0.5$ and 1.0 configurations, respectively, for a given dimensionless heat source protrusion of $s/L = 0.5$. Such a comparison reveals an increase in $\overline{Nu}$ ranging from 5 to 50% as a result of a decrease in b/L. The highest enhancement is at heater 4 for $Re = 10\,000$. As explained previously, this enhancement is due to increased flow velocities in the more constricted channel.

Composite data correlation

With the previous study of the influence of heat source protrusion and wall spacing on the heat transfer in the system, an attempt was made to develop a composite correlation of all experimental data. As has been observed previously, the heat transfer characteristics of heater 1 show a complex dependence on Reynolds number, and no attempt was made to correlate these data for all geometric parameters investigated. However, heaters 2–4 showed effects similar enough to warrant a composite correlation of the form

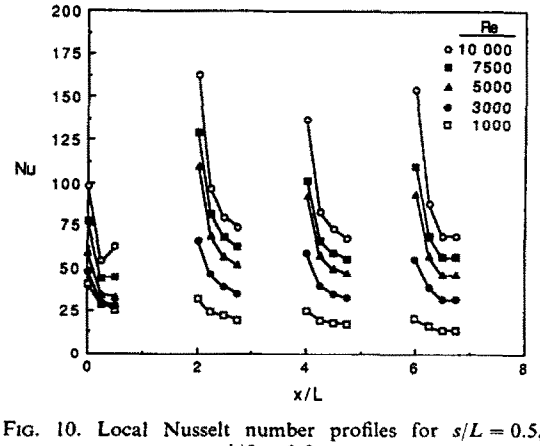

FIG. 10. Local Nusselt number profiles for $s/L = 0.5$, $b/L = 0.5$.

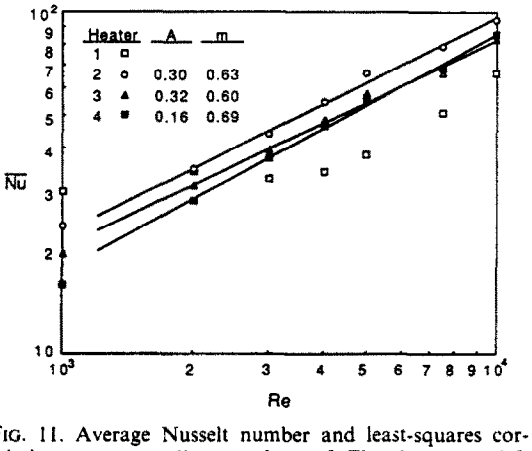

FIG. 11. Average Nusselt number and least-squares correlations corresponding to data of Fig. 10, $s/L = 0.5$, $b/L = 0.5$.

$\overline{Nu} = f(Re, b/L, s/L)$. A similar correlation was also developed for the heater average Nusselt number based on the bulk temperature, defined as

$$\overline{Nu}_b = q_{conv} L/k(\overline{T_w - T_b}). \quad (10)$$

The bulk temperature appearing in equation (10) was calculated from the total heat transfer to the fluid upstream of the designated heater. The value $(\overline{T_w - T_b})$ is the average difference between the local wall temperature and the fluid bulk temperature. In the calculation of $\overline{Nu}_b$, the thermal conductivity was evaluated at the film temperature, $(\overline{T_w + T_b})/2$. Using least-squares regression techniques the average Nusselt number based on T_0 $(\overline{Nu})$, and that based on T_b $(\overline{Nu}_b)$ were correlated using an expression of the form $\overline{Nu} = A\, Re^m (b/L)^n (s/L)^p$. The resulting correlation equations for $\overline{Nu}$ and $\overline{Nu}_b$ were found, respectively, to be

$$\overline{Nu} = 0.244\, Re^{0.61} (b/L)^{-0.40} (s/L)^{0.10} \quad (11)$$

and

$$\overline{Nu}_b = 0.323\, Re^{0.59} (b/L)^{-0.43} (s/L)^{0.10}. \quad (12)$$

The correlation coefficient and average error associated with equation (11) were 0.96 and 8.4%, respectively, while those for equation (12) were found to be 0.96 and 7.6%, respectively. Note that these correlations are valid for $2000 \leqslant Re \leqslant 10\,000$, $0.5 \leqslant b/L \leqslant 1.0$, and $0.5 \leqslant s/L \leqslant 1.0$. These correlations are not valid for flush-mounted heaters, $s/L = 0$, for which data may be found elsewhere [8]. The two correlations are very similar, differing in average Nusselt number by only 6% over the range of parameters studied. The $\overline{Nu}_b$ data for heaters 2–4 and all b/L and s/L studied experimentally are illustrated in Fig. 12, along with the correlation of equation (12). Also shown for comparison is the correlation for $\overline{Nu}$, the average Nusselt number based on the channel inlet temperature, equation (11). The difference in the two correlations is slight in this case because the bulk temperature rise is minimal for the heat fluxes studied here, never exceeding 4°C in all experiments. The correlations reveal a Reynolds number dependence very similar to that found previously of $m = 0.65$ [2, 3]. Additionally, the slight dependence on protrusion height $(s/L)^{0.10}$ is noted, and agrees qualitatively with previous work [6].

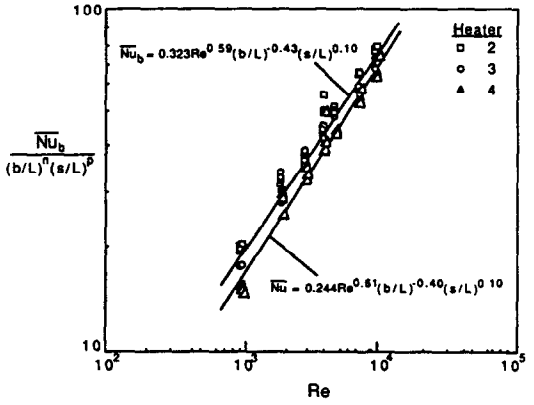

FIG. 12. Correlation of average Nusselt number based on bulk temperature for heaters 2–4, all protruding heat sources and channel wall spacings.

CONCLUSIONS

Local heat transfer coefficients have been measured for forced convective flow over a two-dimensional array of discrete heat sources in the Reynolds number range $1000 \leqslant Re \leqslant 10\,000$. Experiments were performed to investigate the effect of heat source protrusion and channel wall spacing (as measured by the effective flow area). The results show that for flush-mounted heat sources, there is a heat transfer enhancement from heater to heater due to the interruption of the thermal boundary layer in the intervening adiabatic sections separating the heaters. Protrusion of the heat sources results in enhanced heat transfer particularly for the second and subsequent heaters. This is explained by flow separation and associated vena contracta effects, with eventual downstream transition to turbulent flow induced by the presence of the protruding heaters. The local and average Nusselt numbers for the heat transfer prevailing on heaters 2–4 are from 40 to 90% higher than that on heater 1. Flow visualization results corroborated the assertion that the flow separation and the onset of turbulent flow was responsible for the increased heat transfer for protruding heaters, and revealed that these flow structure-altering phenomena occurred first at $Re \approx 2000$. Further heat source protrusion was observed to result in only marginal increases in local and average Nusselt number. Finally, a decrease in the effective flow area as measured by a decrease in the channel wall spacing resulted in increases in both local and average heat transfer. The amount of the increase varied between 5 and 50% for the range of Reynolds number and dimensionless wall spacing investigated.

Acknowledgement—The financial support of the National Science Foundation under Grant No. CBT-8552493 is gratefully acknowledged.

REFERENCES

1. E. M. Sparrow, J. E. Niethammer and A. Chaboki, Heat transfer and pressure drop characteristics of arrays of rectangular modules encountered in electronic equipment, *Int. J. Heat Mass Transfer* **25**, 961–973 (1982).
2. G. L. Lehmann and R. A. Wirtz, Convection from surface mounted repeating ribs in a channel flow, ASME Paper No. 84-WA/HT-88, ASME, New York (1984).
3. G. L. Lehmann and R. A. Wirtz, The effect of variations in stream-wise spacing and length on convection from surface mounted rectangular components. In *Heat Transfer in Electronic Equipment—1985*, pp. 39–47. ASME, New York (1985).
4. R. J. Moffat, D. E. Arvizu and A. Ortega, Cooling electronic components: forced convection experiments

with an air-cooled array. In *Heat Transfer in Electronic Equipment—1985*, pp. 17–27. ASME, New York (1985).
5. R. Moffat and D. E. Arvizu, The use of superposition in calculating cooling requirements for circuit board mounted electronic components, IEEE Paper CH 1781-4/82/0000-b133 (1982).
6. M. J. Chang, R. J. Shyu and L. J. Fang, An experimental study of heat transfer from surface mounted components to a channel airflow, ASME Paper No. 87-HT-75, ASME, New York (1987).
7. C. R. Biber and B. G. Sammakia, Transport from discrete heated components in a turbulent channel flow, ASME Paper No. 86-WA/HT-68, ASME, New York (1986).
8. E. M. Sparrow, A. Garcia and W. Chuck, Turbulent duct flow with streamwise nonuniform heating at the duct wall, *Int. J. Heat Mass Transfer* **30**, 175–185 (1987).
9. J. Davalath and Y. Bayazitoglu, Forced convection cooling across rectangular blocks, *ASME J. Heat Transfer* **109**, 321–328 (1987).
10. Y. Asako and M. Faghri, Three-dimensional heat transfer and fluid flow analysis of arrays of rectangular blocks encountered in electronic equipment, ASME Paper No. 87-HT-78, ASME, New York (1987).
11. R. W. Knight and M. E. Crawford, Simulation of convective heat transfer in pipes and channels with periodically varying cross-sectional area. In *Numerical Methods in Thermal Problems* (Edited by R. W. Lewis, K. Mortan and W. G. Habashi), Vol. 5, pp. 512–523. Pineridge Press, Swansea (1987).
12. R. W. Knight and M. E. Crawford, Numerical prediction of turbulent flow and heat transfer in channels with periodically varying cross sectional area. In *Proc. 1988 National Heat Transfer Conf.* (Edited by H. R. Jacobs), Vol. 1, pp. 669–676. ASME, New York (1988).
13. S. J. Kline and F. A. McClintock, Describing uncertainties in single-sample experiments, *Mech. Engng* 3–12 (January 1953).
14. F. P. Incropera and D. P DeWitt, *Introduction to Heat Transfer*. Wiley, New York (1985).
15. E. M Sparrow and M. M Ohadi, Comparison of turbulent thermal entrance regions for pipe flows with developed velocity and velocity developing from a sharp-edged inlet, *ASME J. Heat Transfer* **109**, 1028–1030 (1988).

TRANSFERT THERMIQUE LOCAL PAR CONVECTION A PARTIR DE SOURCES DISCRETES DE CHALEUR ENCASTREES OU EN SAILLIE

Résumé—Des expériences sont conduites pour mesurer les caractéristiques locales de la convection forcée de chaleur pour un arrangement de sources thermiques discrètes bidimensionnelles. Les nombres de Reynolds relatifs à l'écoulement d'air varient entre 1000 et 10000. On considère des configurations de chauffoirs saillants et aussi deux espacements différents de paroi du canal independamment de la saillie de la source thermique. Des mesures locales de température sont faites le long de la surface chaude parallèle à l'écoulement. Les résultats d'expérience montrent que les sources en saillie donnent des transferts plus élevés que les sources affleurant la surface pour un même nombre de Reynolds. L'interruption de la couche limite dans les sections adiabatiques entre les chauffoirs provoque un accroissement du transfert du chaleur. La saillie de la source de chaleur provoque des flux de chaleur significativement plus élevés pour le second chauffoir si le nombre de Reynolds est supérieur à 2000. Ceci s'explique par l'effet de séparation d'écoulement et de contraction de veine, avec une éventuelle transition vers l'écoulement turbulent en aval comme le montrent des visualisations expérimentales. Des mesures locales révèlent que la variation sensible de la température pariétale entre les faces du chauffoir est fortement affectée par la structure de l'écoulement. Des coefficients moyens de convection calculés par intégration des mesures locales sont présentés en fonction du nombre de Reynolds et des paramètres adimensionnels géométriques étudiés.

ÖRTLICHER WÄRMEÜBERGANG IN ERZWUNGENER KONVEKTION AN HERVORSTEHENDEN UND BÜNDIG ABSCHLIESSENDEN ZWEIDIMENSIONALEN EINZELNEN WÄRMEQUELLEN

Zusammenfassung—Der örtliche Wärmeübergang in erzwungener Konvektion an einer Anordnung von zweidimensionalen einzelnen Wärmequellen wird experimentell untersucht. Die aufgeprägte Luftströmung führt zu effektiven Reynolds-Zahlen im Kanal im Bereich von 1000 bis 10000. Es werden bündig abschließende und überstehende Anordnungen von Wärmequellen untersucht. Außerdem werden zwei unterschiedliche Abstände der Kanalwände verwendet. Die örtlichen Temperaturen an der gleichförmig beheizten Oberfläche werden in Strömungsrichtung gemessen. Die Versuchsergebnisse zeigen, daß die überstehenden Wärmequellen bei gleicher Kanal-Reynolds-Zahl einen besseren Wärmeübergang aufweisen als die bündig abschließenden. Die Unterbrechung der thermischen Grenzschicht in den nichtbeheizten Bereichen zwischen den Wärmequellen führt zu der Erhöhung des Wärmeübergangs. Im Falle der überstehenden Wärmequellen ergibt sich für Kanal-Reynolds-Zahlen oberhalb 2000 eine spürbare Erhöhung des Wärmeübergangs von der ersten Wärmequelle zur zweiten und zu allen weiteren. Dies wird mit einer Strömungsablösung erklärt, wobei möglicherweise in stromabwärtiger Richtung ein Übergang zu turbulenter Strömung stattfindet. Dies wurde bei einer Sichtbarmachung der Strömung festgestellt. Die örtlichen Wärmeübergangsmessungen ergeben merkliche Schwankungen der Wandtemperatur an der beheizten Oberfläche, was stark durch die Struktur der Strömung beeinflußt wird. Eine Integration der örtlichen Meßergebnisse führt zu mittleren Wärmeübergangskoeffizienten, die dann korreliert und als Funktion der Reynolds-Zahl und dimensionsloser geometrischer Parameter dargestellt werden.

ЛОКАЛЬНЫЙ ТЕПЛОПЕРЕНОС ПРИ ВЫНУЖДЕННОЙ КОНВЕКЦИИ ОТ ВЫСТУПАЮЩИХ И УСТАНОВЛЕННЫХ ЗАПОДЛИЦО ДВУМЕРНЫХ ДИСКРЕТНЫХ ИСТОЧНИКОВ ТЕПЛА

Аннотация—Экспериментально определены локальные характеристики теплопереноса при вынужденной конвекции от набора двумерных дискретных источников тепла. Скорости течения воздуха были такими, что обусловливали эффективные значения числа Рейнольдса для канала в диапазоне 1000–10 000. Рассматриваются конфигурации установленных заподлицо и выступающих нагревателей, а также случаи с двумя различными расстояниями между стенками канала независимо от выступа источников тепла. Измерены локальные температуры вдоль однородно нагреваемой поверхности, параллельной направлению течения. Результаты экспериментов показывают, что при постоянном значении числа Рейнольдса для канала теплоперенос от выступающих источников тепла более интенсивен, чем от установленных заподлицо. Разрыв теплового пограничного слоя на адиабатических участках между нагревателями вызывает усиление теплопереноса. Выступ источников тепла способствует значительной интенсификации теплопереноса от второго и последующих нагревателей при значениях числа Рейнольдса для канала свыше 2000. Этот факт объясняется эффектом оторвавшегося потока и сужающейся струи с последующей турбулизацией вниз по течению и экспериментально устанавливается при помощи визуализации течения. Локальные измерения теплопереноса обнаружили существенное изменение температуры стенки на гранях нагревателя, в значительной степени обусловленное структурой течения. Скоррелированы и представлены через число Рейнольдса и безразмерные геометрические параметры средние коэффициенты теплопереноса, рассчитанные методом пространственного интегрирования локальных измерений.